Letter | Editors' Suggestion

Direct imaging of electrical switching of antiferromagnetic Néel order in α-Fe_2O_3 epitaxial films

Egecan Cogulu,[1,*] Nahuel N. Statuto,[1] Yang Cheng,[2] Fengyuan Yang,[2] Rajesh V. Chopdekar,[3] Hendrik Ohldag,[3] and Andrew D. Kent[1]

[1]*Department of Physics, Center for Quantum Phenomena, New York University, New York, New York 10003, USA*
[2]*Department of Physics, The Ohio State University, Columbus, Ohio 43210, USA*
[3]*Advanced Light Source, Lawrence Berkeley National Laboratory, Berkeley, California 94720, USA*

(Received 6 December 2020; revised 8 February 2021; accepted 19 February 2021; published 10 March 2021)

We report the direct observation of switching of the Néel vector of antiferromagnetic (AFM) domains in response to electrical pulses in micron-scale Pt/α-Fe_2O_3 Hall bars using photoemission electron microscopy. Current pulses lead to reversible and repeatable switching with the current direction determining the final state, consistent with Hall effect experiments that probe only the spatially averaged response. Current pulses also produce irreversible changes in domain structure, in and even outside the current path. In both cases only a fraction of the domains switch in response to pulses. Furthermore, the analysis of images taken with different x-ray polarizations shows that the AFM Néel order has an out-of-plane component in equilibrium that is important to consider in analyzing the switching data. These results show that—in addition to effects associated with spin-orbit torques from the Pt layer, which can produce reversible switching—changes in AFM order can be induced by purely thermal effects.

DOI: 10.1103/PhysRevB.103.L100405

The electrical control of antiferromagnetic (AFM) order is a topic of great current interest that has been enabled by recent advances in spintronics, specifically the ability to produce spin currents and spin torques based on spin-orbit interactions [1–4]. AFM states offer advantages compared to those of ferromagnets in that their spin dynamics generally occurs on faster timescales and they are relatively impervious to magnetic fields. They also do not generate macroscopic fields. This makes them both interesting as well as challenging to study as their microscopic spin structure does not produce strong magnetic signatures. Nonetheless, current-induced switching has been reported in AFM thin films using electronic transport signatures (e.g., the Hall effect) to infer domain reorientation [5–14]. However, recent studies of NiO show that such inferences can be equivocal because electromigration can lead to the same transport response as that ascribed to switching of AFM domains [15,16]. Microscopy has been used to study the switching of domains in metallic AFMs [17,18], but there are few reports of such studies on insulating AFM. It is, thus, critical to have more direct information on the AFM domain response to electrical pulses to advance the understanding of their spin dynamics.

In this Letter we use x-ray microscopy to directly observe the AFM domain structure in Pt/α-Fe_2O_3 Hall bars and their response to electrical pulses. Spatially and element-resolved x-ray magnetic linear dichroism (XMLD) photoemission electron microscopy (PEEM) reveals reorientation of the Néel vector where the current flow direction repeatably sets and resets the domain orientation. However, domains outside the current path generally switch irreversibly. In both cases, only a small region near and in the Hall cross switches. Furthermore, our analysis of images taken with different x-ray polarizations reveals an out-of-plane component to the Néel vector in equilibrium, that is, before current pulses are applied to the sample. These results are consistent with switching of the Néel vector between states with in- and out-of-the-plane spin components.

Our experiments were designed to detect the AFM domain structure and changes to this structure in response to current pulses. They were carried out at the PEEM3 beamline 11.0.1.1 of the Advanced Light Source at Lawrence Berkeley National Laboratory in the geometry shown in Fig. 1(a) [19]. X rays were incident at a 30° angle to the film surface and polarized either in the plane of incidence, labeled π polarization (blue arrow), or perpendicular to this plane, labeled σ polarization (red arrow). In this configuration, σ polarization is completely in the film plane, whereas π polarization is at an angle of 60° to the film plane. Moreover, the energy of the incoming photons were resonant with the Fe L_{2a} and L_{2b} edges making their absorption dependent on the magnetic order [20–22] (see Fig. S1 in the Supplemental Material [23]). The XMLD response, thus, allows characterization of the AFM order both in—with σ- polarization—and out-of-the-film plane with π-polarization x rays. The XMLD contrast is typically a few percent, which is easily detectable with PEEM.

The experiments were performed on 30-nm-thick epitaxial α-Fe_2O_3 grown on single crystalline c-axis-oriented Al_2O_3 substrates at 500 °C using off-axis sputtering [10]. The films were capped *in situ* with a 2-nm Pt layer deposited at room temperature. Electron-beam lithography and ion milling were used to pattern the Pt layer into six-legged Hall cross structures with 1-μm linewidth Pt leads. The Hall-cross structure was oriented such that the Pt leads coincide with the three easy

*egecancogulu@nyu.edu

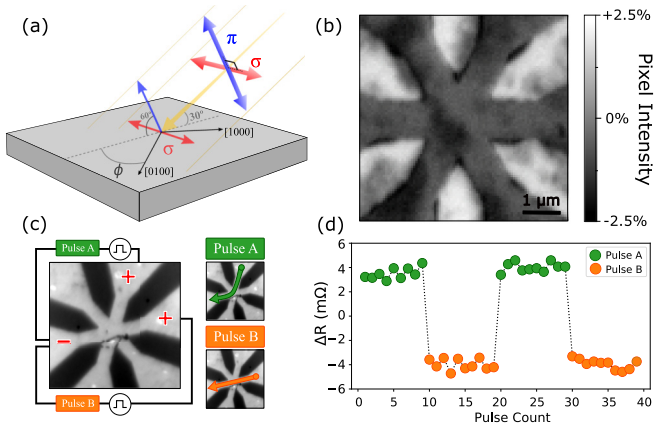

FIG. 1. (a) Schematic of the experimental setup showing the two incident x-ray polarizations σ and π and their projections on the sample. The sample was rotated by a small azimuthal angle ϕ so that the [1000] and [0100] crystal axes have different projections along π and σ polarizations. (b) XMLD-PEEM image of the six-legged Hall cross with AFM domains visible both on bare Fe_2O_3 regions (lighter regions) and under the 2-nm-thick Pt layer (darker regions). The scale bar indicates the percentage contrast, relative to the background. (c) Left: PEEM image with a schematic of the circuit. Bright regions correspond to Pt-covered areas, and dark regions correspond to bare Fe_2O_3. Pulses were applied from "+" to the ground "−" for both pulse generators. Right: pulse *A* and pulse *B* panels show the current paths for each pulse. The dark line at the bottom of the central part of the Hall cross is a cut disconnecting the two bottom leads from the current path. (d) Transverse resistance measurements in response to 4-mA and 10-ms pulses *A* and *B* on a sister sample with the bottom leads connected. See Fig. S4 in the Supplemental Material for the measurement configuration [23].

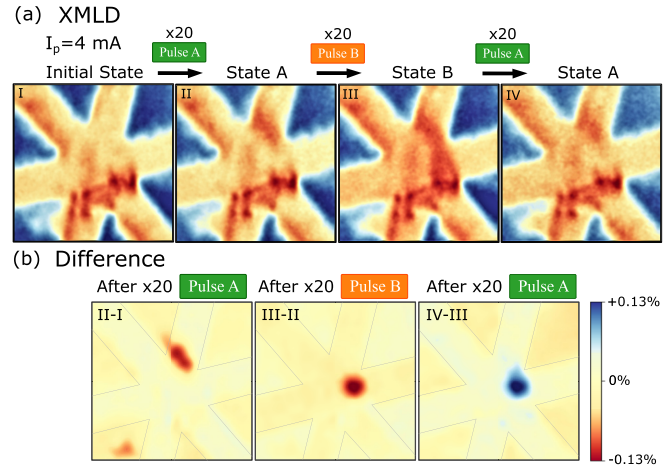

FIG. 2. AFM domain changes in response to current pulses. (a) XMLD images showing a 4×4-μm^2 field of view. Image I shows the sample before the current is applied; images II–IV are images taken after the application of 20 current pulses of type *A*, type *B*, and then type *A*, respectively. The pulse amplitude is 4 mA for all the images in the sequence. (b) Differences of XMLD images in panel (a) to highlight the pulse-induced changes to the AFM domain structure. The color scale in (b) is expanded to highlight changes.

in-plane axes ([1000],[0100],[0010]) of the *c*-axis-oriented α-Fe_2O_3 [10]. Figure 1(b) shows a XMLD-PEEM image of the sample. The darker regions are covered with the thin Pt layer, and the brighter regions are where Pt is etched, exposing the α-Fe_2O_3 surface. AFM domains are observed in both regions. Their boundaries are gray-to-black contrast changes in the Pt-covered regions and the white-to-gray transitions in the α-Fe_2O_3-exposed regions. The lateral scale of the domains is $\sim$1 μm, and domains extend between the two regions.

To characterize the orientation of the Néel vector, XMLD images were acquired as a function of the sample orientation ϕ in Fig. 1(a). XMLD contrast depends on the *magnitude* of the projection of the x-ray polarization $\hat{p}$ on the Néel vector $\hat{n}$, $(\hat{p} \cdot \hat{n})^2$. Therefore, for in-plane oriented spins, XMLD images are invariant under a 180° sample rotation for both σ and π polarizations. Based on the spin structure and studies of α-Fe_2O_3 thin films, we expected the Néel vector to be oriented along in-plane easy-axis directions [10,11,24] and, thus, that both sets of images would be invariant under 180° sample rotation.

However, surprisingly, our results show that for π polarization, the image contrast changes significantly on 180° rotation. The σ-polarization images return to the same contrast levels on rotation as expected. This indicates that, in addition to having different in-plane projections, the AFM Néel vector at the sample surface is appreciably canted out of the film plane, which may reflect an interface perpendicular magnetic anisotropy or be an effect of strain induced by the lattice mismatch between the film and the substrate. See Fig. S3 in the Supplemental Material for the results of the sample rotation experiments [23].

The effect of electrical pulses on the AFM domain structure was studied by applying currents to the Hall bar *in situ*, with the sample in the PEEM microscope. Prior electrical studies have shown that the current flow direction leads to different transverse (Hall) voltages that were associated with changes in the AFM domain structure [10,11]. Thus, we configured the sample to enable current pulses to be applied in two different directions. Figure 1(c) shows the sample layout with connections to two separate pulse generators, labeled *A* and *B*. The images on the right of Fig. 1(c) show the current directions for *A* and *B* pulses.

Samples were also characterized electrically prior to XMLD PEEM experiments. Current pulses were applied, and the transverse voltage was measured. The data shown in Fig. 1(d) are for 4-mA amplitude 10-ms duration pulses. After each pulse a small sensing current 100 μA ($\ll$4 mA) was used to measure the transverse voltage. The data points are color coded according to the pulse type. As reported previously, there is a step change in voltage when going from *A*- to *B*-type pulses as well as going from *B*- to *A*-type pulses [10]. Furthermore, subsequent pulses of the same type do not change the transverse voltage.

Figure 2(a) shows a sequence of four XMLD images taken before and after applying current pulses. They show the difference in the electron yield for σ and π polarizations to maximize the signal originating from AFM order. Blue regions are bare Fe_2O_3, and red/orange regions correspond to the Pt leads. The field of view is 4×4 μm^2. Image I shows the initial domain configuration before pulses were applied. Images II–IV show the states after sending a sequence of 20

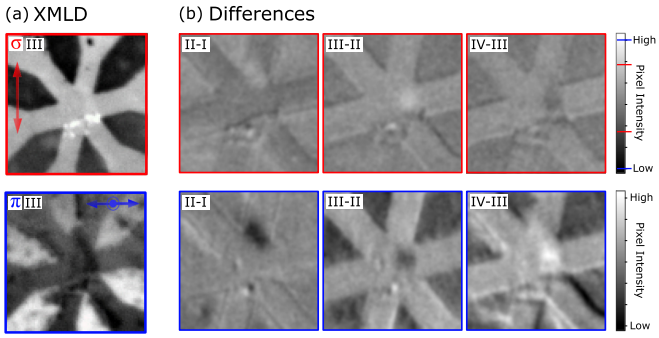

FIG. 3. (a) σ and π projections of Image III in Fig. 2(a). Bright regions indicate that the AFM order is aligned perpendicular to the polarization direction whereas dark regions indicate that the AFM order aligns parallel to the polarization direction. (b) σ (top panel) and π (bottom panel) projections of the difference images in Fig. 2(b). The same scale bar is used on both panels to highlight the larger contrast in the π polarization images. The marks on the σ color scale bar show the maximum and minimum values for σ (red marks) and π (blue marks) polarization difference images.

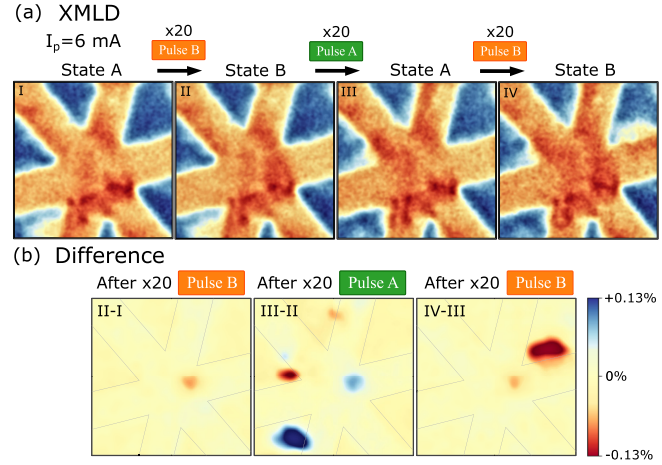

FIG. 4. AFM domain response to larger amplitude current pulses. (a) Image I shows the initial sample state which is State A. It is followed by images II, III and IV taken after $20 \times B$ pulses, $20 \times A$ pulses and $20 \times B$ pulses, respectively. In each case the current amplitude was 6 mA. (b) Differences of XMLD images in panel (a) highlight the pulse-induced changes with an expanded color scale, the same as that of Fig. 2(b).

of the same pulse type, first pulse A, then B, and then A again. The labels State A and State B above the images correspond to the preceding pulse type. Changes in AFM order correspond to color changes between subsequent images. For example, in Image II there is added contrast in the pulse A positive lead after 20 type-A pulses and in Image III a domain to the right of the center of the Hall cross has reoriented after 20 type-B pulses. Whereas in Image IV, after A pulses, this domain has returned to its initial configuration.

To bring out the changes in AFM domain structure we show difference images in Fig. 2(b). In these images blue regions represent positive contrast changes, and red regions represent negative contrast changes. The color map is chosen to highlight the current-induced changes; the black lines indicate the boundaries of the Pt leads. The II-I image clearly shows the domain that has reoriented in response to the first set of A pulses is in one of the current leads to the Hall cross. Image III-II shows the domain that has switched in the Hall cross area in response to B pulses. After another set of A pulses, the contrast returns to that after the first set of A pulses, State A, the state shown in Fig. 2(a)II.

From these results, we identify two types of domain changes in response to current pulses: (1) reversible changes, regions that go back and forth between State A and State B after the corresponding pulses; and (2) irreversible regions in which the domain configuration does not return to its initial state. The reversible changes occur in regions in which the current density is large and its flow direction changes significantly between that of pulses A and B (see Fig. S5 in the Supplemental Material for the current flow directions [23]). In both cases, it is also clear that the Néel vector of only a fraction of the domains in the current path change their orientation in response to pulses.

To determine the changes in the orientation of the Néel vector induced by current pulses we now analyze data from the σ- and π-polarization images separately. Figure 3(a) shows the σ- and π-polarization data that are used to form Image III in Fig. 2(a).

The σ polarization is in the film plane and, thus, provides sensitivity to changes in the projection of the Néel vector on this plane, whereas the π polarization has both in and out of the film plane projections. In these images, bright contrast in a region indicates that the AFM order is mostly aligned perpendicular to the polarization direction, whereas dark contrast indicates that the AFM order aligns mostly parallel to the polarization direction. Although the contrast associated with the switched AFM domain is visible in both polarization images, the contrast is much stronger in the π-polarization images. Moreover, dark contrast of the AFM switched region in the π-polarization image indicates that the projection of the Néel vector on the π polarization has changed significantly in response to the current pulse.

We now separately analyze the polarization dependence of the difference images in Fig. 2(b). The results are shown in Fig. 3(b). The top row of images (red bordered images) shows the σ-difference images that highlight changes to the in-plane AFM order. The lower row of blue-bordered images show the π-difference images that are sensitive to the projection on the π-polarization direction. All six difference images are on the same color scale to be able to compare the changes in contrast. The contrast change in π-polarization images is approximately twice as large as that of the σ-polarization images. This indicates that the projection of the Néel vector on the π polarization changes more than its projection on the σ-polarization direction.

We further studied the effect of higher currents. We repeated the same pulse sequences as in Fig. 2 but this time with a 50% higher current pulse amplitude 6 mA. Figure 4(a) shows XMLD images taken before and after applying the current pulses. Starting from State A [Fig. 2(a)II] and applying 20 current pulses of B, then A, and then B again. Figure 4(b) shows the differences between images, again to highlight the change in domain structure associated with the current pulses. Figure 4(b) shows the differences between the images, again

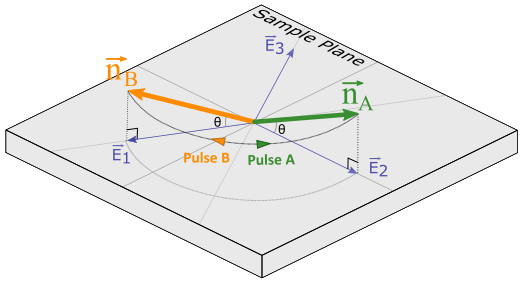

FIG. 5. Schematic of the switching of the Néel vector between easy-axis directions that cant out of the film plane, which is consistent with both the XMLD-PEEM results and the Hall response. $\vec{n}_A$ and $\vec{n}_B$ are the orientations of the Néel vector after pulse *A* and pulse *B*, respectively. The dotted lines with arrows show the switching direction of the Néel vector in response to the pulses. These arrows associated with pulse *A* and pulse *B* correspond to blue and red changes, respectively, in the difference images in Figs. 2(b) and 4(b).

to highlight the change in domain structure associated with the current pulses.

Besides the fact that the reversible domain reorientation is still observable, the light blue dot in Fig. 4(b), at this larger current there are additional changes. In difference panels (III-II) and (IV-III) blue and red regions represent new AFM domains switched by the application of pulse *A* and that most of them are irreversible switches. In contrast to Fig. 2 where almost all the switched AFM domains were in the current path, Fig. 4(b) shows switched regions outside of the current path. In fact, the blue region in panel (III-II) is situated well outside the region that experiences the current.

Previous work on current-induced switching in α-Fe_2O_3 assumes that the Néel vector lies and rotates completely in the film [10,11]. However, our sample characterization and polarization-dependent analysis show that this is not the case. The fact that the contrast of the AFM domains changes in the π-projection images after a 180° rotation combined with the fact that we are observing more contrast in the π-polarization images indicate that the Néel vector has an equilibrium out-of-plane component. Our results show that the current-induced switching is between easy axes that are canted out of the film plane as indicated in Fig. 5. The canting angle of the Néel vector can be determined by doing the rotation experiment discussed in the Supplemental Material [23] with more polarizations and more sample orientations ϕ. The data from this study allow us to put a lower limit of 30° on the canting angle. The mechanism for the canting is currently unclear, although interfacial effects resulting from the Pt layer or strain may play a role.

Now in the light of these observations, we turn to the question of the potential switching mechanisms. Two main mechanisms were used to explain the observed magnetoresistance, spin-orbit torques (SOT), and thermally induced magnetostriction. For the spin-orbit-torque case, the spin accumulation generated in the Pt acts as an effective magnetic field and exerts a dampinglike SOT on the Néel order to align it with the current direction. Whereas for thermally induced magnetostriction, compressive normal stresses induced by Joule heating changes the anisotropy energy through magnetostriction, thus, also favoring alignment of the Néel vector with the applied current. In easy-plane antiferromagnets with large magnetostrictive coefficients, such as α-Fe_2O_3 and NiO, this can outweigh dampinglike torques [11,25]. Our finite element simulations (see Figs. S6 and S7 in the Supplemental Material [23]) show that both the current density levels ($\sim 2 \times 10^8$ A/cm^2) and the thermally induced compressive normal stresses are above their respective required thresholds (~50 MPa) to induce switching. This suggests that both mechanisms potentially contribute to the switching. The fact that we can see changes in the Néel vector outside of the current path demonstrates that thermally induced magnetostriction alone is enough to produce switching since there cannot be any SOT effects where there is no current. However, we also see all of the reversible domain changes in the current flow path, i.e., where SOT is present.

To conclude, we directly imaged repeatable current-induced switching of antiferromagnetic moments in α-Fe_2O_3/Pt bilayers with XMLD-PEEM. We observed that only a fraction of the domains reorient, consistent with electrical measurements—which shows that the Hall effect response is less than that expected for complete switching in the Hall cross region. We further identified two types of response that tend to occur in different regions: reversible switches in the Hall cross area and irreversible switches in and outside the Hall cross. Although both SOT and thermally induced magnetostriction potentially contribute to switching, our experiments with high current density pulses demonstrate that thermal effects alone can induce changes in the Néel order by showing there are irreversible changes to the AFM domain structure outside the electrical path. To gain further insights into the switching mechanisms, the impacts of SOT and thermal effects on AFM order need to be separated, such as by electrically (but not thermally) isolating the metal layers from the α-Fe_2O_3, or using light metals (e.g., Al) instead of Pt, which will be the topics of future studies.

This research was supported by the Air Force Office of Scientific Research under Grant No. FA9550-19-1-0307. The nanostructures were realized at the Advanced Science Research Center NanoFabrication Facility of the Graduate Center at the City University of New York. This research also used resources of the Advanced Light Source, a U.S. DOE Office of Science User Facility under Contract No. DE-AC02-05CH11231. Beamline 11.0.1.1 was used for XMLD-PEEM imaging, and Beamline 6.3.1 was used for magnetic spectroscopy.

[1] V. Baltz, A. Manchon, M. Tsoi, T. Moriyama, T. Ono, and Y. Tserkovnyak, Antiferromagnetic spintronics, Rev. Mod. Phys. **90**, 015005 (2018).

[2] I. M. Miron, K. Garello, G. Gaudin, P.-J. Zermatten, M. V. Costache, S. Auffret, S. Bandiera, B. Rodmacq, A. Schuhl, and P. Gambardella, Perpendicular switching of a single

ferromagnetic layer induced by in-plane current injection, Nature (London) **476**, 189 (2011).

[3] L. Liu, C.-F. Pai, Y. Li, H. W. Tseng, D. C. Ralph, and R. A. Buhrman, Spin-torque switching with the giant spin Hall effect of tantalum, Science **336**, 555 (2012).

[4] A. Hoffmann, Spin Hall effects in metals, IEEE Trans. Magn. **49**, 5172 (2013).

[5] P. Wadley, B. Howells, J. Železny, C. Andrews, V. Hills, R. P. Campion, V. Novak, K. Olejnik, F. Maccherozzi, S. S. Dhesi, S. Y. Martin, T. Wagner, J. Wunderlich, F. Freimuth, Y. Mokrousov, J. Kune, J. S. Chauhan, M. J. Grzybowski, A. W. Rushforth, K. W. Edmonds, B. L. Gallagher, and T. Jungwirth, Electrical switching of an antiferromagnet, Science **351**, 587 (2016).

[6] X. Z. Chen, R. Zarzuela, J. Zhang, C. Song, X. F. Zhou, G. Y. Shi, F. Li, H. A. Zhou, W. J. Jiang, F. Pan, and Y. Tserkovnyak, Antidamping-Torque-Induced Switching In Biaxial Antiferromagnetic Insulators, Phys. Rev. Lett. **120**, 207204 (2018).

[7] M. Meinert, D. Graulich, and T. Matalla-Wagner, Electrical Switching of Antiferromagnetic Mn_2Au and the Role of Thermal Activation, Phys. Rev. Appl. **9**, 064040 (2018).

[8] X. F. Zhou, J. Zhang, F. Li, X. Z. Chen, G. Y. Shi, Y. Z. Tan, Y. D. Gu, M. S. Saleem, H. Q. Wu, F. Pan, and C. Song, Strong Orientation-Dependent Spin-Orbit Torque in Thin Films of the Antiferromagnet Mn_2Au, Phys. Rev. Appl. **9**, 054028 (2018).

[9] S. Yu. Bodnar, L. Šmejkal, I. Turek, T. Jungwirth, O. Gomonay, J. Sinova, A. A. Sapozhnik, H.-J. Elmers, M. Kläui, and M. Jourdan, Writing and reading antiferromagnetic Mn_2Au by Néel spin-orbit torques and large anisotropic magnetoresistance, Nat. Commun. **9** (2018).

[10] Y. Cheng, S. Yu, M. Zhu, J. Hwang, and F. Yang, Electrical Switching of Tristate Antiferromagnetic Néel Order in α-Fe_2O_3 Epitaxial Films, Phys. Rev. Lett. **124**, 027202 (2020).

[11] P. Zhang, J. Finley, T. Safi, and L. Liu, Quantitative Study on Current-Induced Effect in an Antiferromagnet Insulator/Pt Bilayer Film, Phys. Rev. Lett. **123**, 247206 (2019).

[12] T. Moriyama, K. Oda, T. Ohkochi, M. Kimata, and T. Ono, Spin torque control of antiferromagnetic moments in NiO, Sci. Rep. **8**, 14167 (2018).

[13] L. Baldrati, O. Gomonay, A. Ross, M. Filianina, R. Lebrun, R. Ramos, C. Leveille, F. Fuhrmann, T. R. Forrest, F. Maccherozzi, S. Valencia, F. Kronast, E. Saitoh, J. Sinova, and M. Kläui, Mechanism of Néel Order Switching in Antiferromagnetic Thin Films Revealed by Magnetotransport and Direct Imaging, Phys. Rev. Lett. **123**, 177201 (2019).

[14] I. Gray, T. Moriyama, N. Sivadas, G. M. Stiehl, J. T. Heron, R. Need, B. J. Kirby, D. H. Low, K. C. Nowack, D. G. Schlom, D. C. Ralph, T. Ono, and G. D. Fuchs, Spin Seebeck Imaging of Spin-Torque Switching in Antiferromagnetic Pt/NiO Heterostructures, Phys. Rev. X **9**, 041016 (2019).

[15] C. C. Chiang, S. Y. Huang, D. Qu, P. H. Wu, and C. L. Chien, Absence of Evidence of Electrical Switching of the Antiferromagnetic Néel Vector, Phys. Rev. Lett. **123**, 227203 (2019).

[16] A. Churikova, D. Bono, B. Neltner, A. Wittmann, L. Scipioni, A. Shepard, T. Newhouse-Illige, J. Greer, and G. S. D. Beach, Non-magnetic origin of spin Hall magnetoresistance-like signals in Pt films and epitaxial NiO/Pt bilayers, Appl. Phys. Lett. **116**, 022410 (2020).

[17] S. Y. Bodnar, M. Filianina, S. P. Bommanaboyena, T. Forrest, F. Maccherozzi, A. A. Sapozhnik, Y. Skourski, M. Kläui, and M. Jourdan, Imaging of current induced Néel vector switching in antiferromagnetic Mn_2Au, Phys. Rev. B **99**, 140409(R) (2019).

[18] T. Janda, J. Godinho, T. Ostatnicky, E. Pfitzner, G. Ulrich, A. Hoehl, S. Reimers, Z. Šobáň, T. Metzger, H. Reichlová, V. Novák, R. P. Campion, J. Heberle, P. Wadley, K. W. Edmonds, O. J. Amin, J. S. Chauhan, S. S. Dhesi, F. Maccherozzi, R. M. Otxoa, P. E. Roy, K. Olejník, P. Němec, T. Jungwirth, B. Kaestner, and J. Wunderlich, Magneto-seebeck microscopy of domain switching in collinear antiferromagnet CuMnAs, Phys. Rev. Mater. **4**, 094413 (2020).

[19] A. Doran, M. Church, T. Miller, G. Morrison, A. T. Young, and A. Scholl, Cryogenic PEEM at the advanced light source, J. Electron Spectrosc. Relat. Phenom. **185**, 340 (2012).

[20] P. Kuiper, B. G. Searle, P. Rudolf, L. H. Tjeng, and C. T. Chen, X-Ray Magnetic Dichroism Of Antiferromagnet Fe_2O_3: The Orientation Of Magnetic Moments Observed By Fe 2p X-Ray Absorption Spectroscopy, Phys. Rev. Lett. **70**, 1549 (1993).

[21] A. Scholl, Observation of antiferromagnetic domains in epitaxial thin films, Science **287**, 1014 (2000).

[22] S. Park, H. Jang, J.-Y. Kim, B.-G. Park, T.-Y. Koo, and J.-H. Park, Strain control of morin temperature in epitaxial α-Fe_2O_3 (0001) film, Europhys. Lett. **103**, 27007 (2013).

[23] See Supplemental Material at https://link.aps.org/supplemental/10.1103/PhysRevB.103.L100405 for details on XMLD image processing, rotation experiments, and finite element simulations.

[24] A. H. Morrish, *Canted Antiferromagnetism: Hematite* (World Scientific, Singapore, 1995).

[25] H. Meer, F. Schreiber, C. Schmitt, R. Ramos, E. Saitoh, O. Gomonay, J. Sinova, L. Baldrati, and M. Kläui, Direct imaging of current-induced antiferromagnetic switching revealing a pure thermomagnetoelastic switching mechanism, Nano Lett. **21**, 114 (2021).